JOURNAL OF GEOPHYSICAL RESEARCH, VOL. 110, C03020, doi:10.1029/2004JC002377, 2005

Observations of internal bores and waves of elevation on the New England inner continental shelf during summer 2001

Mark Pritchard
Institute for Atmospheric Science, School of Earth and Environment, University of Leeds, Leeds, UK

Robert A. Weller
Department of Physical Oceanography, Woods Hole Oceanographic Institute, Woods Hole, Massachusetts, USA

Received 10 March 2004; revised 13 December 2004; accepted 27 January 2005; published 23 March 2005.

[1] During July–August 2001, oceanographic variability on the New England inner continental shelf was investigated with an emphasis on temporal scales shorter than tidal periods. Mooring and ship survey data showed that subtidal variation of inner shelf stratification was in response to regional Ekman upwelling and downwelling wind driven dynamics. High-frequency variability in the vertical structure of the water column at an offshore mooring site was linked to the baroclinic internal tide and the onshore propagation of nonlinear solitary waves of depression. Temperature, salinity, and velocity data measured at an inshore mooring detected a bottom bore that formed on the flood phase of the tide. During the ebb tide, a second bottom discontinuity and series of nonlinear internal waves of elevation (IWOE) formed when the water column became for a time under hydraulic control. A surface manifestation of these internal wave crests was also observed in aircraft remote sensing imagery. The coupling of IWOE formation to the offshore solitary waves packets was investigated through internal wave breaking criterion derived in earlier laboratory studies. Results suggested that the offshore solitons shoaled on the sloping shelf, and transformed from waves of depression to waves of elevation. The coupling of inshore bore formation to the offshore solitary waves and the possible impact of these periodic features on mixing on the inner shelf region are discussed.

Citation: Pritchard, M., and R. A. Weller (2005), Observations of internal bores and waves of elevation on the New England inner continental shelf during summer 2001, *J. Geophys. Res.*, *110*, C03020, doi:10.1029/2004JC002377.

1. Introduction

[2] The waters of the New England continental shelf have strong seasonal variability in the stratification of the water column. During the late spring and summer months, stratification is established through positive surface heat fluxes, and a strong seasonal thermocline forms at depths of approximately 20 m [*Lentz et al.*, 2003]. Our aim here is to examine this summertime variability at tidal periods and shorter as observed close to shore on the continental shelf south of Martha's Vineyard, Massachusetts.

[3] In general, the stratification of inner New England waters is modified through mixing and restratification by wind-driven flows associated with synoptic meteorological variability, diurnal period forcing in insolation, sea breeze, and tidal currents. Typically, through late summer, the New England shelf is forced by winds from the southwest for periods of up to 5 to 6 days which favor weak upwelling conditions along the coast.

[4] Mean and seasonal subtidal geostrophic currents on the New England shelf, south of Martha's Vineyard (see Figure 1), are westward along isobaths supported by across-isobath temperature gradients [*Shearman and Lentz*, 2003]. Subtidal current variability is also seen in wind-driven currents responding locally to synoptic weather events. Semi-diurnal tidal flows can in turn give rise to further variability in the temperature structure of the inner shelf through the generation of solitary waves on the pycnocline [*Shearman and Lentz*, 2004].

[5] Interaction of the tidal flow with bottom topography can form the solitary waves that propagate away from the source and then may evolve into internal bores [*Holloway*, 1987; *Lamb*, 1994; *Lamb and Yan*, 1996]. In situ observations and remote sensing with Synthetic Aperture Radar (SAR) have pointed to the formation of nonlinear internal waves at shelf breaks [*Lee and Beardsley*, 1974; *Apel et al.*, 1995; *Stanton and Ostrovsky*, 1998]. The Shelfbreak Primer study on the New England shelf suggested tidal currents advecting stratified fluid over steep topography onto the inner shelf region as the cause of soliton generation [*Colosi et al.*, 2001].

[6] High-frequency variability of stratification in shallower waters may also occur through onshore internal wave propagation. *Klymack and Moum* [2003] observed solitary waves of elevation on the Oregon shelf at depths of

0148-0227/05/2004JC002377$09.00

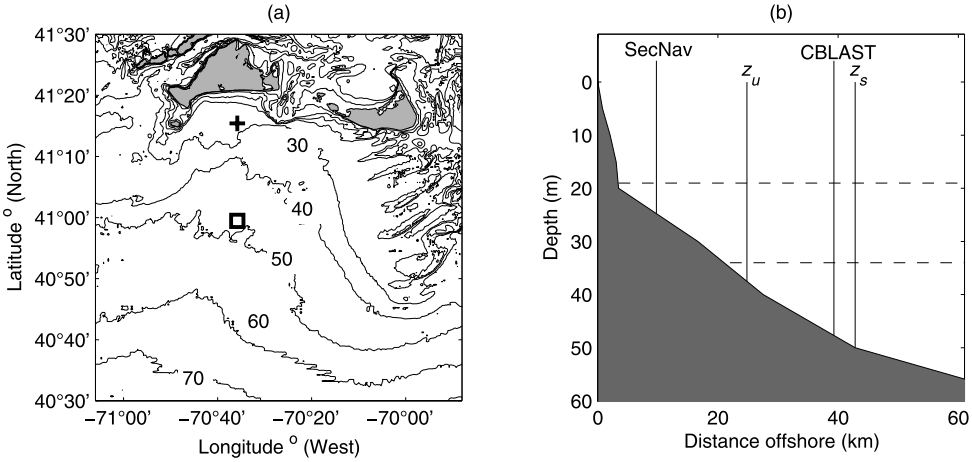

Figure 1. Geographical location and across-shelf bathymetry of the study area. (a) Position of SecNav (plus sign) and CBLAST (square) moorings. (b) Across-shelf bathymetry showing relative positions of each moorings and theoretical positions of internal wave shoaling (z_s) and instability (z_u).

approximately 120 m. The series of high-amplitude waves of O(22 m) were formed due to the almost two-layer stratification on the shelf.

[7] *Helfrich* [1992] examined solitary internal waves propagating into much shallower water over sloping topography in the laboratory. Results showed that as the solitary wave shoaled, it broke, and evolved into a series of turbulent surges and ''boluses'' that continued to propagate up the slope. As the upslope surge retreated under gravitational relaxation, it collided with secondary incoming waves, producing a series of nonlinear waves of elevation.

[8] Nearshore observations made by *Winant* [1974] in water shallower than 20 m suggested that internal wave-like perturbations in the vertical structure of the water column shoreward to the outer surf zone resulted from the shoaling processes as described by *Helfrich* [1992]. Further observations made by *Pineda* [1999] describe breaking internal waves running up into the surf zone followed by offshore propagation of a bore-like surface feature.

[9] Our goal for this study using high temporal resolution mooring data was to investigate higher frequency variations in summertime seasonal stratification of a shallow inner shelf water column at periods shorter than tidal. We interpret several periodic series of high-frequency perturbations in water column properties superimposed on top of regional coastal Ekman dynamics as nonlinear internal waves driven by the internal tide. These internal waves which originate from the outer shelf are shown to change polarity from internal waves of depression to internal waves of elevation across the gentle slope of the inner shelf region. In waters less than 30 m deep, these elevated internal waves further interact with ebb tidal flows and possible gravitationally driven instabilities. Finally, we discuss the likely impact of such observed high-frequency wave-like features on well-stratified inner shelf dynamics.

2. Observational Methods

[10] In the summer of 2001, two sites south of Martha's Vineyard (Figure 1) were occupied with moorings as part of the Coupled Boundary Layer Air-Sea Transfer low winds (CBLAST-LOW) pilot experiment [*Pritchard et al.*, 2002]. The offshore surface mooring, labeled as CBLAST, was in place at 40°59.46′N, 70°35.85′W in 47 m of water from 17 July to 18 August 2001 (year days 198–230). A pair of moorings, one subsurface and one surface that provided real time telemetry of data through the entire water column, labeled as SecNav, was deployed at 41°15.43′N, 70°35.23′E in 27 m of water from 30 July to 18 August 2001 (year days 211–230). Diagrams of the moorings are shown in Figure 2. Both surface buoys were equipped to collect surface meteorological data.

[11] The subsurface instrumentation on CBLAST (Figure 2a) included 29 Onset Tidbit temperature recorders sampling every 10 min, 10 Seabird SBE-37 temperature and conductivity loggers sampling every 30 s, and a 600 KHz RDI Workhorse ADCP sampling 100 ping (second) burst every 5 min. In addition to a surface mooring, a Seabird SBE-26 tide gauge was deployed near the CBLAST mooring site. Tidal elevation levels were computed every 10 min from bottom pressure and density records from the tide gauge and corrected with respect to atmospheric pressures recorded by the CBLAST mooring ASIMET meteorological data.

[12] The SecNav surface mooring (Figure 2b) carried six Seabird SBE-39 temperature recorders and six SBE-37 temperature and conductivity recorders all sampling every 30 s and three Sontek Argonaut-MD acoustic Doppler current meters sampling every minute; the subsurface mooring carried two SBE-37 temperature and conductivity recorders and two SBE-39 temperature recorders all sampling every 30 seconds and one Sontek Argonaut-MD current meter sampling every minute (Figure 2b). Tidal elevation was estimated from pressure sensors incorporated into the SBE-37 temperature and conductivity recorders on the subsurface mooring. More detail about the moorings and instrumentation is provided by *Pritchard et al.* [2002].

[13] In addition to mooring data, three across-shelf and one along-shelf surveys of temperature and salinity structure were completed using a Seabird SBE-19 CTD. Pre- and post-calibrations and quality control analyses were carried

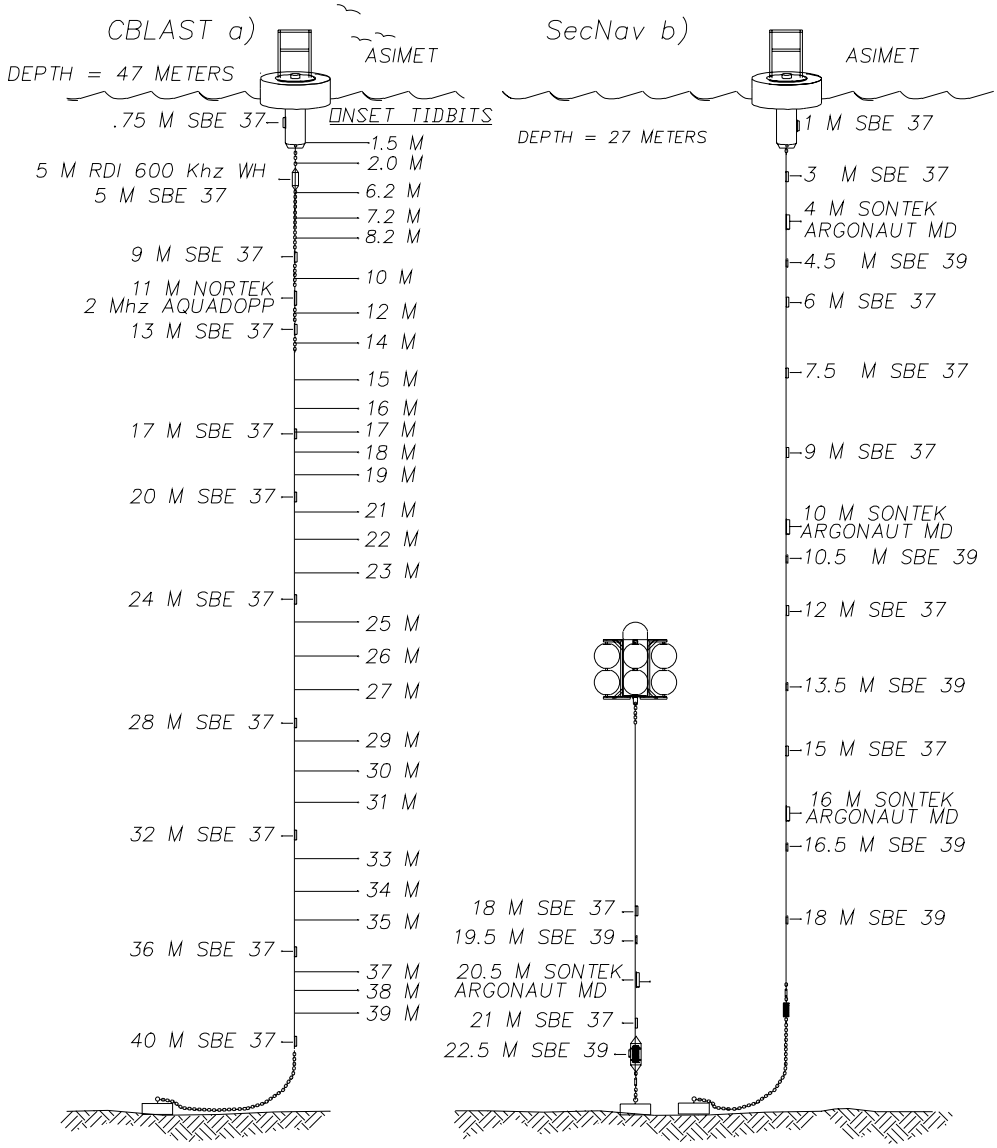

Figure 2. Schematic diagrams of instrumentation deployed on the (a) CBLAST and (b) SecNav moorings during the 2001 CBLAST-Low pilot experiment.

out and full length records were recovered from all instruments used in this investigation.

3. Regional and Subtidal Inner Shelf Ocean Variability

[14] Through the duration of the two moorings deployment, buoy meteorological data showed that the magnitude of the wind speed (Ws_{mag}) varied in response to regional synoptic weather conditions. Wind speeds peaked at 8.9 m s^{-1} at CBLAST and 6.9 m s^{-1} at SecNav while averaging over the deployment periods of 4.2 m s^{-1} at CBLAST and 5 m s^{-1} at SecNav. These mainly light to moderate winds originating from the west/west-northwest were directionally upwelling favorable for the New England shelf region. The response of inner shelf waters to upwelling favorable winds is shown in Figure 3 through results from three across-shelf CTD transects. The transects recorded between 23 and 25 July 2001 (year day 204–207) ran due south from a station in 9 m of water inshore of the SecNav buoy to just offshore of the CBLAST buoy in 50 m of water.

[15] The developing across-shelf temperature structure shows how cooler waters in the lower water column are gradually forced onshore and begin to rise in response to the wind-driven surface Ekman flow. By year day 207, upwelling response produces a strong well-defined thermocline at a depth of approximately 15 m.

[16] A further more detailed time series of top to bottom water column temperature, salinity, and density anomalies and the magnitude and direction of wind forcing at the CBLAST and SecNav sites is summarized in Figure 4. The data used to investigate water column structure at each mooring site in response to wind-driven forcing were the hourly averaged buoy wind speed data and the shallowest and deepest SBE-37 records on each respective mooring (see Figure 2a and Figure 2b mooring diagrams).

[17] Vertical anomalies at the CBLAST mooring site remained reasonably steady during year day 200–207.

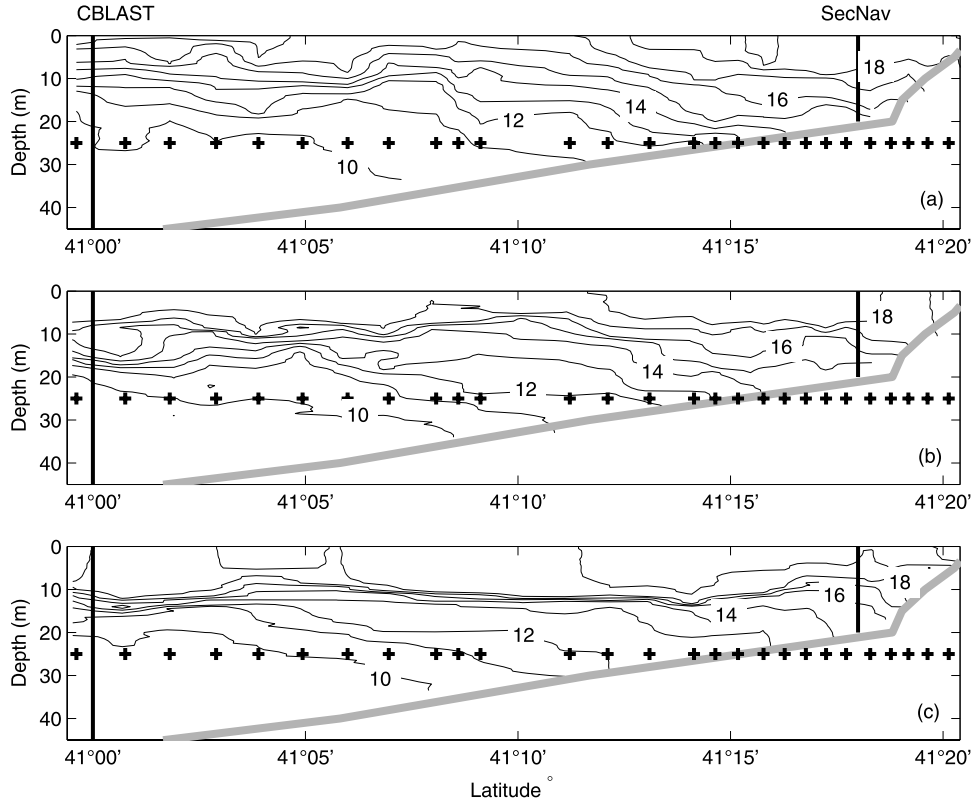

Figure 3. Across-shelf temperature sections from CTD casts made between the CBLAST and SecNav mooring sites. (a) July 23, (b) July 24, and (c) July 25 2001 (year day 204–207). Across-shelf section ran from north to south on a transect parallel with the two moorings. Plus signs mark the positions of the CTD casts.

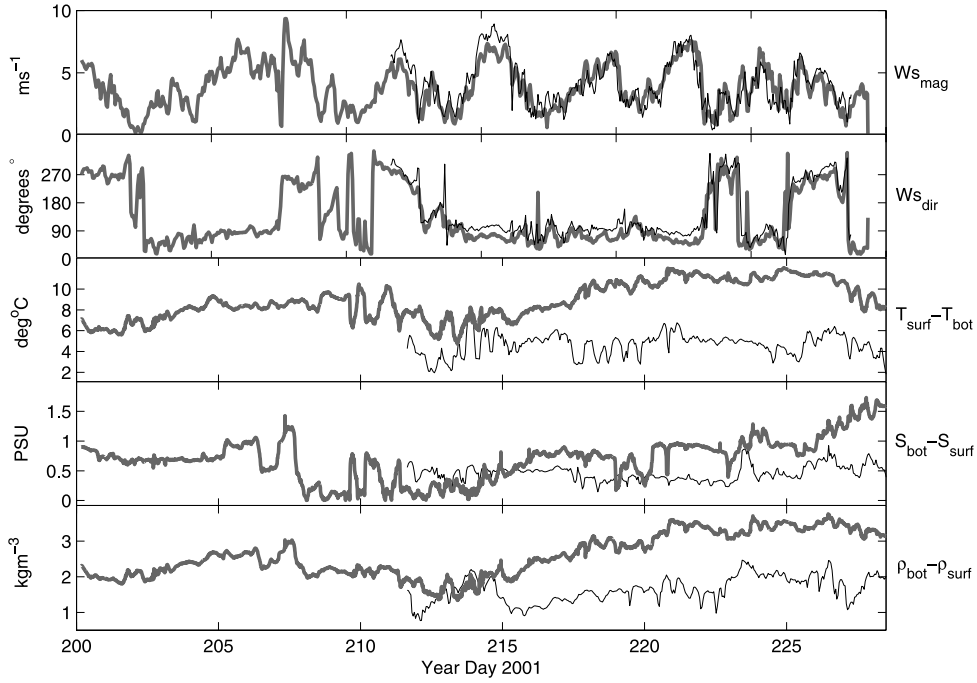

Figure 4. Hourly averaged: wind speed magnitude (Ws_{mag}); wind direction (Ws_{dir}); surface to bottom temperature ($T_{surf} - T_{bot}$), salinity ($S_{bot} - S_{surf}$), and density ($\rho_{bot} - \rho_{surf}$) anomalies at the CBLAST (shaded lines) and SecNav (black lines) mooring sites through their respective deployment periods.

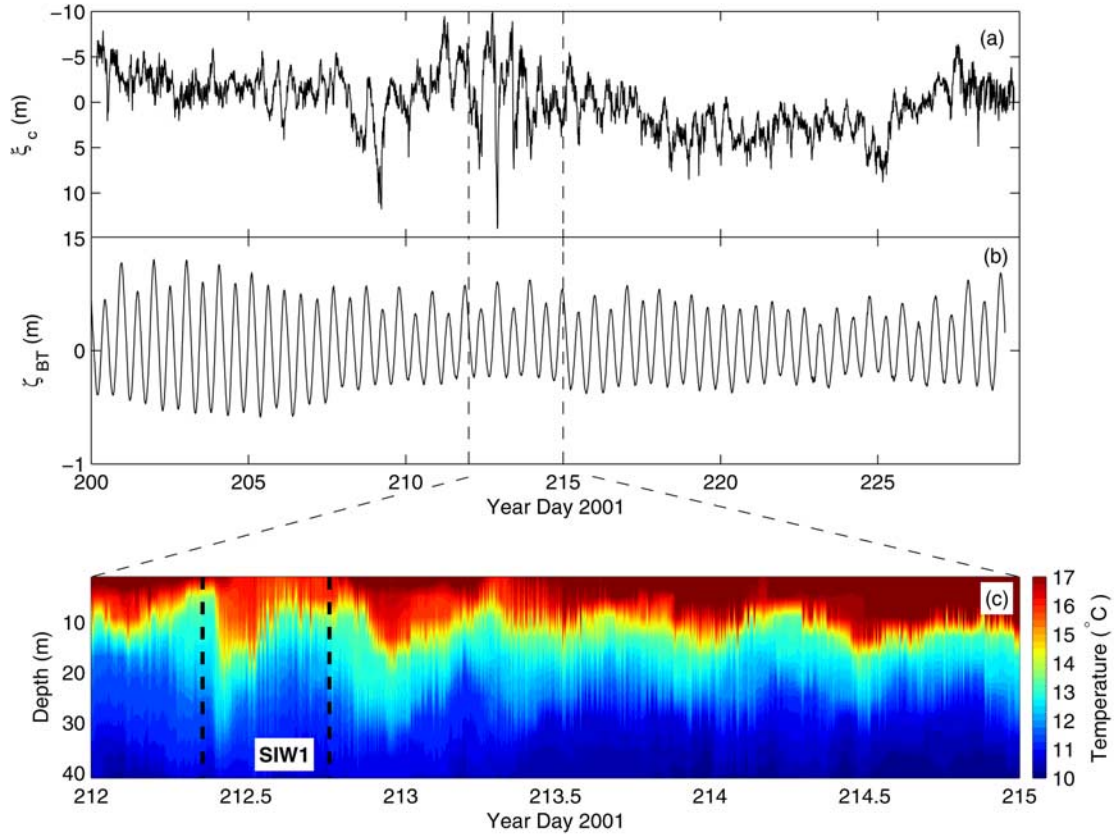

Figure 5. Time series data of (a) vertical 13°C isotherm displacement ξ_c, (b) tidal elevation ζ_{BT}, and (c) temperature between year day 212 and 215 at the CBLAST mooring site.

The salinity anomaly then abruptly decreased to nearly zero and remained low until approximately year day 215. This sudden homogenization of salinity through the water column corresponded to a backing of the wind from a westerly to easterly direction. This effectively disrupted the upwelling type coastal circulation and caused a transition to downwelling transport on the shelf. Thus, higher saline surface waters were being forced onshelf through the mooring site. The time series observations showed that downwelling favorable conditions continued during the period of easterly directed winds until the latter part of year day 212.

[18] Higher southeasterly wind speeds at the time of the SecNav moorings deployment (year day 212) were accompanied by a decrease in the surface to bottom temperature ($T_{surf} - T_{bot}$) and density ($\rho_{bot} - \rho_{surf}$) anomalies at the inshore site. Offshore, the higher downwelling favorable winds were less important to the overall structure of the water column. Figure 4 shows that when high values of Ws_{mag} were directed toward the northwest, $T_{surf} - T_{bot}$ and $\rho_{bot} - \rho_{surf}$ at the inshore site decreased by 4°C and 1.3 kg m^{-3}, respectively. Through this period of downwelling, there was no obvious divergence in SST or surface salinity. Therefore the observed changes to the stratification were being caused by changes in the absolute temperature and salinity of the lower water column. These results suggested that surface waters under the influence of Ekman downwelling dynamics were effectively being transported onshore. Continuity constraints then forced warmer water down at the coast, deepening the thermocline through a mean offshore transport in the lower water column.

[19] As winds backed from southeasterly to northwesterly, the larger-scale coastal circulation quickly readjusted in $O(1/f) \approx 2.89$ hours and became upwelling favorable. From year day 212.5–215, Ws_{mag} dropped to levels of instrument detection threshold. $\rho_{bot} - \rho_{surf}$ at the SecNav site during this period of intense heating was at times >2 kg m^{-3} at year day 214 and then began to role off as Ws_{mag} increased at year day 214.75. The observed increases in $T_{surf} - T_{bot}$ and $\rho_{bot} - \rho_{surf}$ were in response to upwelling and caused the thermo/pycnocline to rise through the ingress of cooler bottom water onshore. From year day 215 through to 221.75, $T_{surf} - T_{bot}$ and $\rho_{bot} - \rho_{surf}$ were relatively constant during low wind periods of <2 m s^{-1}. The sudden observed increase in $\rho_{bot} - \rho_{surf}$ at year day 223.5 at the SecNav mooring was due to an abrupt decrease in surface salinity from 31.6 to 31.1 PSU. The source of this freshwater influx at the inshore site was an unknown but assumed to be either from riverine discharge in Connecticut, west of the study region, or from local groundwater discharge [*Lentz et al.*, 2003; R. K. Shearman, personal communication, 2002].

[20] At year day 225, wind speed again began to decrease and an abrupt warming of the surface layer followed. By year day 226 the winds backed, and became downwelling favorable, causing the observed decrease in $T_{surf} - T_{bot}$.

[21] Results from this analysis demonstrate that the inner shelf at the CBLAST site remained well stratified through

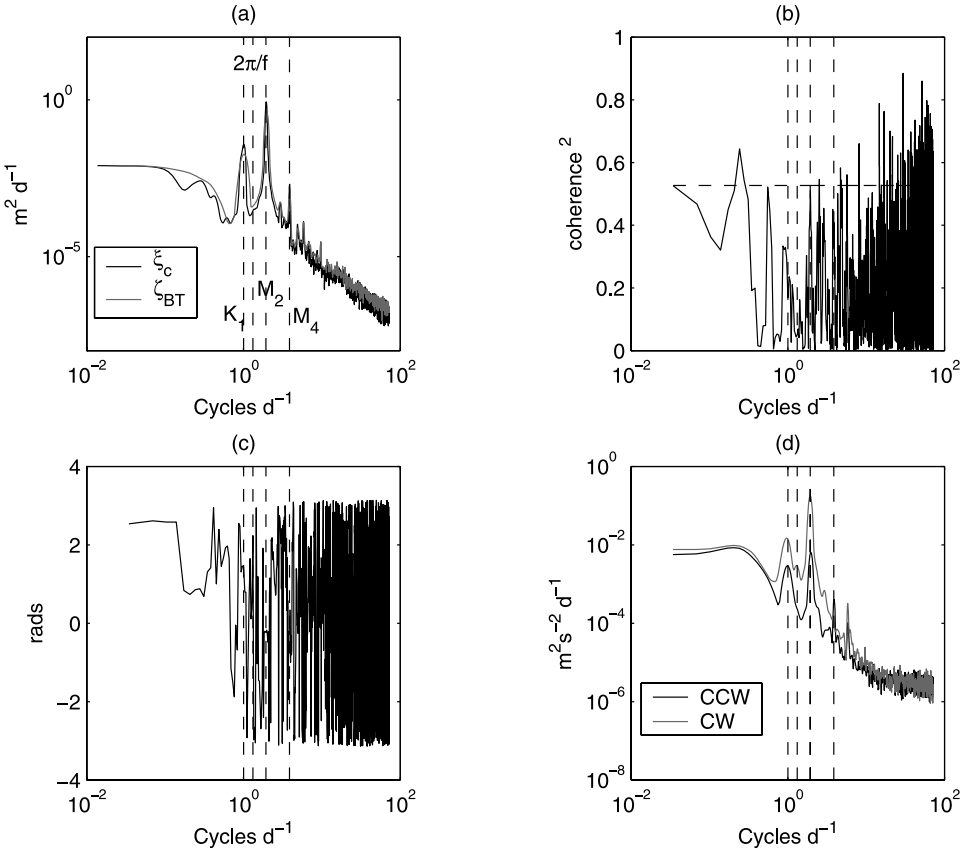

Figure 6. Variance preserving spectral analysis of CBLAST mooring data. (a) Power spectra of isotherm displacement ξ_c and tidal elevation ζ_{BT}. (b) Coherence^2 between ξ_c and ζ_{BT} plus 95% confidence level. (c) Phase relationship between ξ_c and ζ_{BT}. (d) Rotary power spectra of the depth-averaged baroclinic velocities, $\bar{u}_{BC} + i\bar{v}_{BC}$.

the study period. Conversely, stratification at the SecNav site was far more susceptible to coastal Ekman upwelling and downwelling dynamics. Hence the summertime shelf wide stratified conditions that extended all the way into shallow nearshore waters potentially provided a rich environment for the propagation and or formation of internal wave fields.

4. Offshore Internal Waves

[22] *Colosi et al.* [2001] showed the onshore propagation of the internal tide and solitons some 90 km offshore from the CBLAST mooring site. Similar occurrences of nonlinear waveforms are also reported by *MacKinnon and Gregg* [2003] farther inshore. During the duration of our 2001 mooring deployments, strong internal tide signatures were also recorded, approximately 40 km offshore in 47 m of water. Figure 5c shows an example of time series temperature data recorded at the CBLAST site.

[23] The magnitude of vertical isotherm displacement (ξ_c) from an equilibrium level at the CBLAST mooring site was estimated using the shallowest stable isotherm (13°C) from the moorings temperature data. Figure 5a shows ξ_c throughout the CBLAST moorings deployment plotted with respect to a depth of 16 m. The largest displacements occurred on periodic semi-diurnal timescales and consistent with onshore propagation of an internal tidal wave. The maximum amplitude (a_0) of ξ_c during the observational period was in a range of 15 and 20 m. Internal tidal waves of similar amplitude and displacement were observed in previous studies of the New England shelfbreak region [*Colosi et al.*, 2001].

[24] Results from the spectral analysis of ξ_c are presented in Figure 6a. Variance preserving energy spectra show high levels of energy in frequency bands associated with tidal signals. The M_2 and S_2 peaks are centered on 2 cpd but evidence of diurnal, K_1 and beat period variability, 0.63 cpd (between M_2, 1.9 cpd, and the local inertial band, $2\pi/f \approx$ 1.3 cpd), was also found through the upper water column.

[25] Power spectra of local tidal elevation, ζ_{BT} (see Figure 5b), recorded by the tide gauge at the mooring site shown in Figure 6a also illustrated strong semi-diurnal and diurnal tidal signals. However, the results from cross-spectral analysis of ξ_c and ζ_{BT} shown in Figure 6b suggested insignificant coherence between the semi-diurnal bands of the barotropic tides and the vertical oscillations of the thermocline. This result was also reflected in the phase coherence between the two signals shown in Figure 6c that emphasizes the onshelf decoupling of the internal baroclinic and shelf barotropic tides.

[26] Rotary power spectra of the depth-averaged baroclinic currents, $\bar{u}_{BC} + i\bar{v}_{BC}$, recorded at the CBLAST mooring site are shown in Figure 6d. The baroclinic currents were computed by removing the depth-averaged

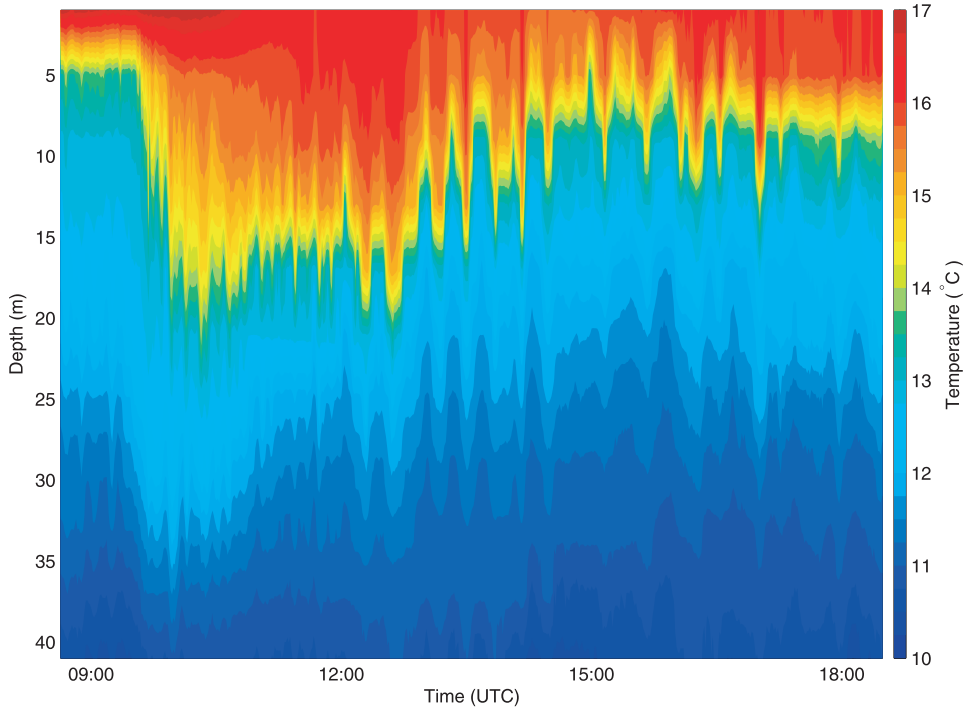

Figure 7. Time series of vertical temperature from 0900–1800 UTC on year day 212, 2001 (SIW1), during passage of nonlinear solitary wave packets at the CBLAST mooring site.

barotropic current, $u_{BT} + iv_{BT}$ from the velocity time series. Again, strong spectral peaks were found at the semi-diurnal tidal band and also at the K_1 diurnal and the wind-driven inertial band (1.3 cpd) in the clockwise component of depth-independent currents. The depth mean M_2 baroclinic tidal ellipses computed from the M_2 tidal constituents derived from the harmonic least squares tidal analysis of $\bar{u}_{BC} + i\bar{v}_{BC}$ velocity data were aligned across shelf (13°T), nearly orthogonal to the 50-m isobath. These results suggest that the observed depth variability of the upper ocean mixed layer was associated with internal tides, atmospheric forcing, and a combination of the two at beat frequencies. Higher-frequency triad nonlinear self interaction of the M_2 tide as reported by *Rippeth and Inall* [2002] on the Malin shelf was also evident at M_4 and M_6 periods in both isotherm and velocity records but was minimal compared to the M_2 tide and wind-driven processes.

[27] An example of a series of solitary waves (SIW1, Figure 5c) observed between 0900 and 1800 UTC on year day 212 is presented in Figure 7. Temperature time series data showed an abrupt deepening of the upper stratified layer followed by several lower amplitude quasi-rank ordered (periodicity ≈ 20 min) solitary internal waves (SIW).

[28] The bulk characteristic density structure (σ_t) and buoyancy frequency, $N_0^2 = (-g/\rho)(\partial\rho/\partial z)$, of the water column computed from a 30-min average of mooring data before and after the passage of SIW1 is shown in Figure 8. The highest N_0^2 values prior to passage of the internal tides wave front were above the 6 m level (20 cph) and deepened to 16 m through passage of the trailing solitary waveforms.

[29] The SIW linear (c_0) and nonlinear (c_1) phase speeds of SIWs observed during year day 212 were estimated from a two-layer linear and Korteweg-de Vries (KdV) model that assumes a balance between weak nonlinearity (α) and weak dispersion (β) and results in the formation of SIWs [e.g., *Holloway*, 1987].

$$c_0 = \left(g \frac{\Delta\rho}{\rho_2} \frac{h_1 h_2}{h_1 + h_2} \right)^{\frac{1}{2}}, \tag{1}$$

$$\alpha = \frac{3c_0(h_2 - h_1)}{2h_1 h_2}, \tag{2}$$

$$\beta = \frac{c_0 h_1 h_2}{6}, \tag{3}$$

$$c_1 = c_0 \left(1 + \frac{a_0 \alpha}{3c_0} \right). \tag{4}$$

[30] The results of solutions to equations (1)–(4) for SIWs and variables illustrated in Figures 7 and 8 are shown in Table 1. Linear (c_0) and nonlinear phase speed (c_1) estimates were within 18% for the examples of wave packets shown, suggesting that the nonlinear modification was small for the observed SIWs.

[31] The length scale of the solitons were then estimated from

$$L^2 = \frac{4}{3} \frac{h_1^2 h_2^2}{(h_1 - h_2) a_0}. \tag{5}$$

[32] Solving for L in equation (5) gives a characteristic wavelength scale corresponding to approximately half the width of the solitary wave ($\text{sech}^2(1) \approx 0.42$). Hence, for the example under consideration during SIW1, wave-

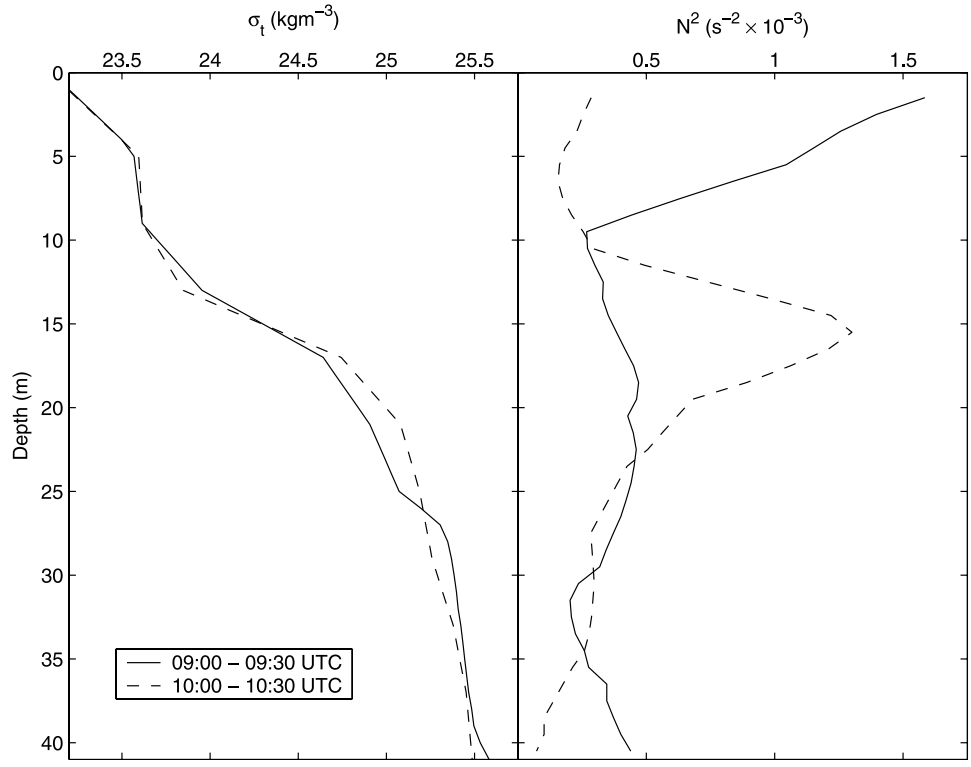

Figure 8. Bulk characteristic density structure (σ_t) and buoyancy frequency (N_0^2) before and after the passage of the SIW1 at the CBLAST mooring during SIW1.

length, $\lambda = 3.6L = 95$ m. Secondary estimates using the nonlinear phase speeds and $\Delta t \approx 10$ min from mooring data spanning a wave of depression gave 192 m.

[33] The discrepancy between methods of wavelength estimation are likely due to the assumptions made of the two-layer KdV model. For example, *Orr and Mignerey* [2003] showed that on a shallowing shelf region, SIWs tended to broaden and were a likely precursor for a SIW polarity reversal from waves of depression to waves of elevation. Nevertheless, this analysis, although not definitive, serves to illustrate the order of change in wavelength properties observed at the CBLAST mooring as compared to those waves observed farther inshore.

5. Inshore Internal Bores and Waves of Elevation

[34] Subsurface instrumentation at the inshore SecNav mooring site also detected internal wave activity and bore formation at tidal frequencies throughout the deployment period. However, in stark contrast to the offshore observations, the vertical excursions of isotherms were in the form of internal waves of elevation (IWOE). In the following sections we discuss our observations in context of both a hydraulic analysis and a conceptual model that incorporates the implication of across-shore tidal advection, gravitational instabilities, and the coalescence flows associated with internal bores and IWOE.

[35] Figure 9a shows an example of temperature time series recorded from 0500–1400 UTC on year day 213. Mooring instrumentation initially displays the propagation of a positively polarized wave front at approximately 0600 UTC that coincided with the time of local low water (see Figure 13b in section 5.1). Temperature time series illustrates the sudden influx of cooler off-shelf water concurrent with the discontinuity. This eventually caused a shallowing of the upper and deepening of the lower layers of the water column. A second bore shown in more detail in Figure 9b formed at the mooring site some 3 hours later. However, in this second instance the bore was trailed in time by a series of quasi-rank ordered IWOEs with amplitudes and period of order 15 m (as measured from the seabed) and 6.5 min, respectively.

[36] Simultaneous Long-EZ aircraft flights on year day 213 that carried an IR imager used to detect small changes in sea surface temperature of $O(0.1°C)$ captured the temperature "slicks" associated with the convergence/divergence zone between the internal waves crest and trough [*Zappa and Jessup*, 2005]. Figure 10 shows an example of

Table 1. Linear and Nonlinear (KdV) Internal Solitary Wave Characteristics Observed During SIW1, Year Day 212, 2001, at the CBLAST Mooring Site

Parameter	Value
h_1	16 m
h_2	31 m
a_0	15 m
$\Delta\rho$	1.4 kg m^3
α	0.012 s^{-1}
β	22.11 m^{3}s^{-1}
c_0	0.27 m s^{-1}
c_1	0.33 m s^{-1}

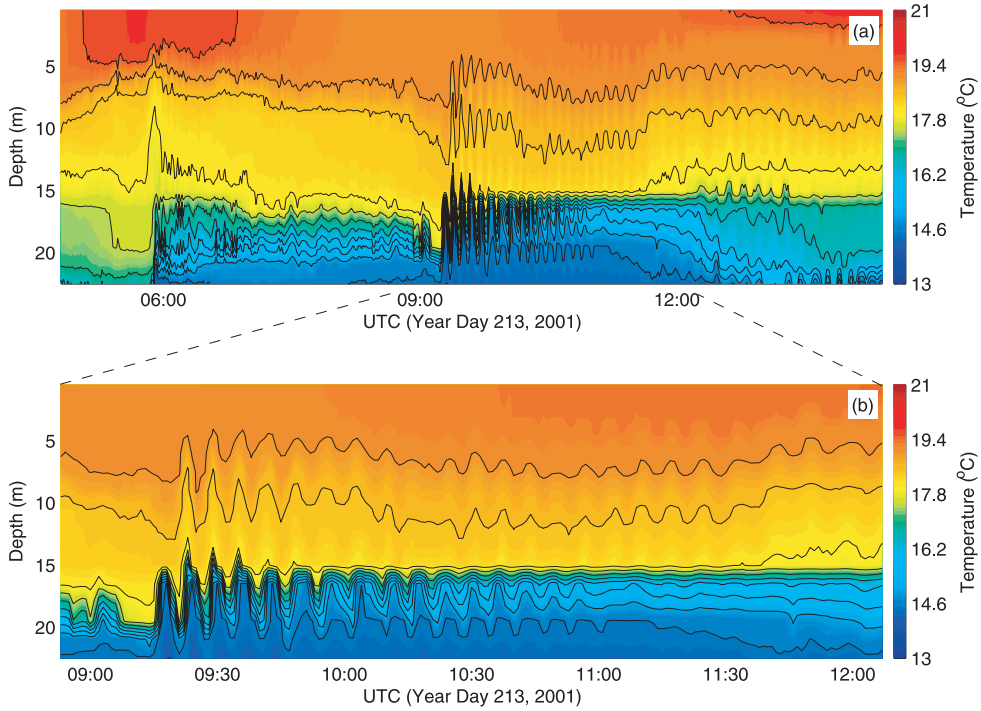

Figure 9. Time series of vertical temperature series of internal bore and nonlinear wave at the SecNav mooring site on year day 213, 2001, (a) 0500–1400 UTC and (b) 0900–1200 UTC for time of passage of nonlinear waves and internal bores at the SecNav mooring site.

an IR image taken before sunrise on 1 August 2001. The IR image was captured from an altitude of 191 m above sea level, and the image size is approximately 100 m × 100 m. During this period, wind speed was below 2 m s^{-1} and directed toward the southeast (see Figure 4). The image shows the internal waves as a series of cooler $O(0.2°C)$ temperature anomalies or surface slicks aligned roughly parallel with local isobaths. Scaling of the IR images suggested the cooler surface temperature slicks were spaced over a distance of approximately 20–40 m.

5.1. Internal Bore and IWOE Dynamics

[37] At the start of the flood tide, the baroclinic across-shelf velocity, v_{BC}, shown in Figure 11 at the 20.5 m level recorded an onshore surge of approximately 15 cm s^{-1}. This abrupt increase in onshore flow was in apparent response to the passage of the internal bore. On the approach to local high water, v_{BC} began to weaken. In contrast, the along-shelf baroclinic velocity, u_{BC}, shown in Figure 12 illustrated strong fluctuations in the flow coincidental with sharp changes in the temperature of the lower water column. Following local high water, the vector sum of baroclinic flows, $U_{BC} = u_{BC} + iv_{BC}$ (see Figure 13a), in the lower water column were on order of only a few cm s^{-1}. However, the vertical velocity, w, in the lower 16 m of the water column as shown in Figure 14 increased. Eventually, the lower layer of the water column began to shallow and ultimately returned to its original depth (upper layer deepens) until the onset of next flood tide. Further occurrences of this same phenomena were seen on several other occasions during the SecNav moorings deployment.

[38] The effects of bore propagation on the bulk stability of the water column at the SecNav site were estimated through a hydraulic control criterion. This approach to the flow and stability analysis at the SecNav site was

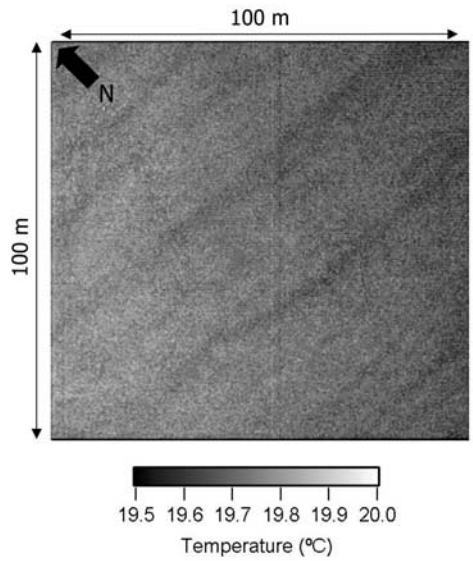

Figure 10. IR images of sea surface temperature recorded by an aircraft flight at an altitude of 191 m at the SecNav mooring site (depth 27 m) on 1 August 2001 (year day 213). The darker slicks indicate cooler water. Figure is modified after *Zappa and Jessup* [2005].

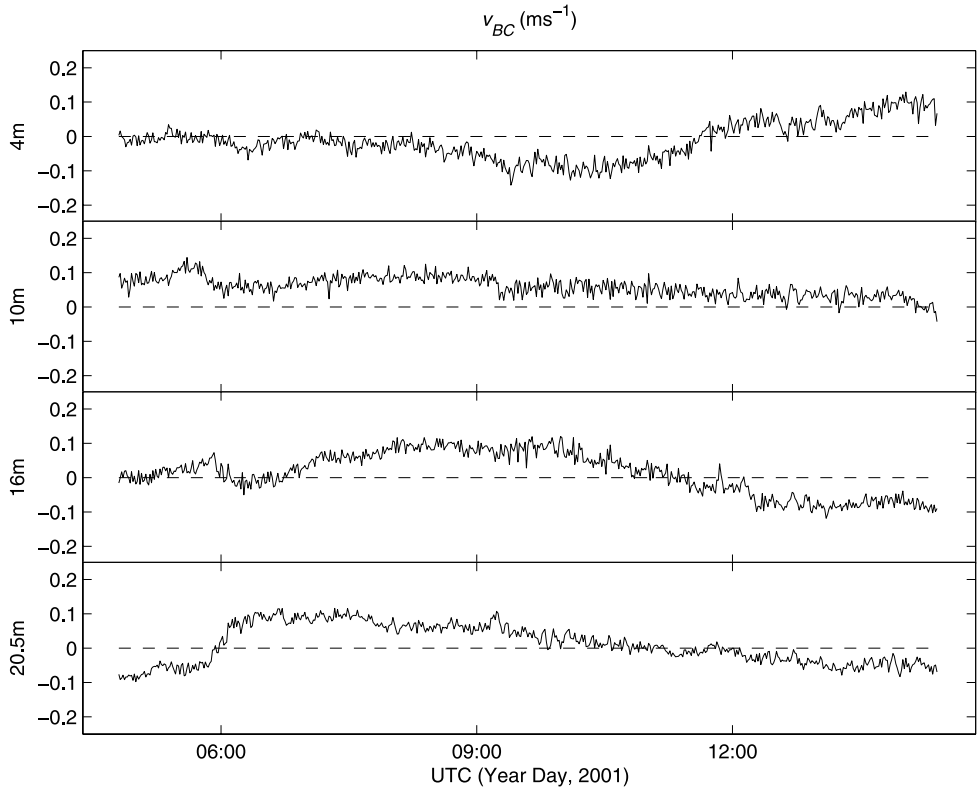

Figure 11. Baroclinic across-shelf velocity, v_{BC}, at four levels in the water column from 0500–1400 UTC on year day 213, 2001, at the SecNav mooring site.

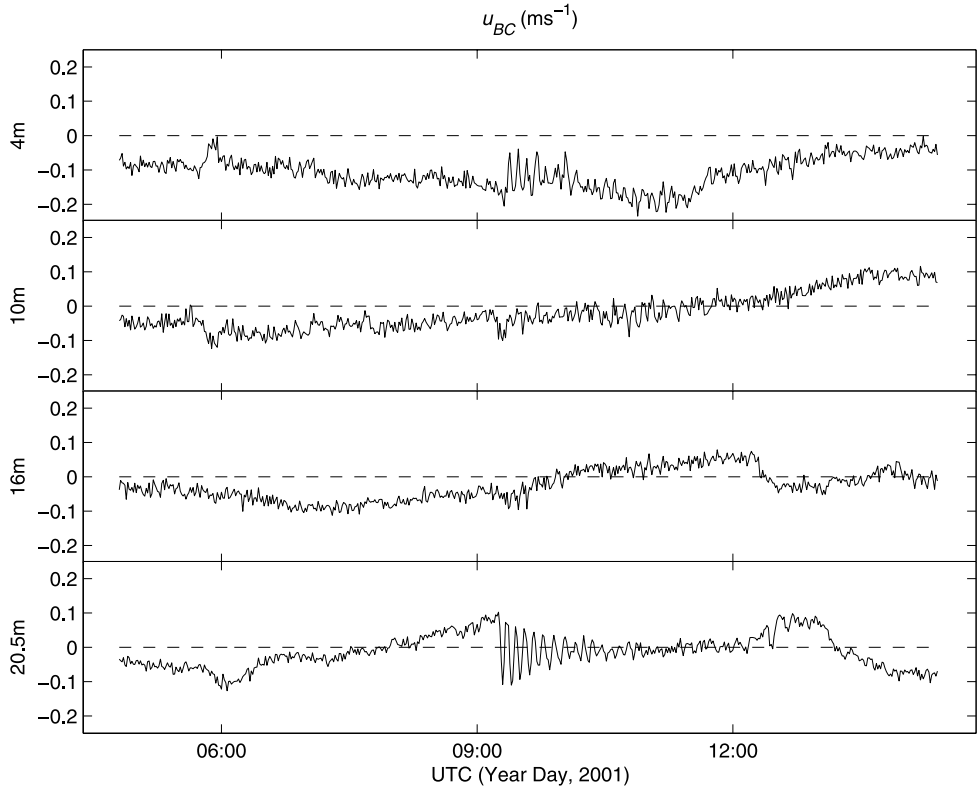

Figure 12. Baroclinic along-shelf velocity, u_{BC}, at four levels in the water column from 0500–1400 UTC on year day 213, 2001, at the SecNav mooring site.

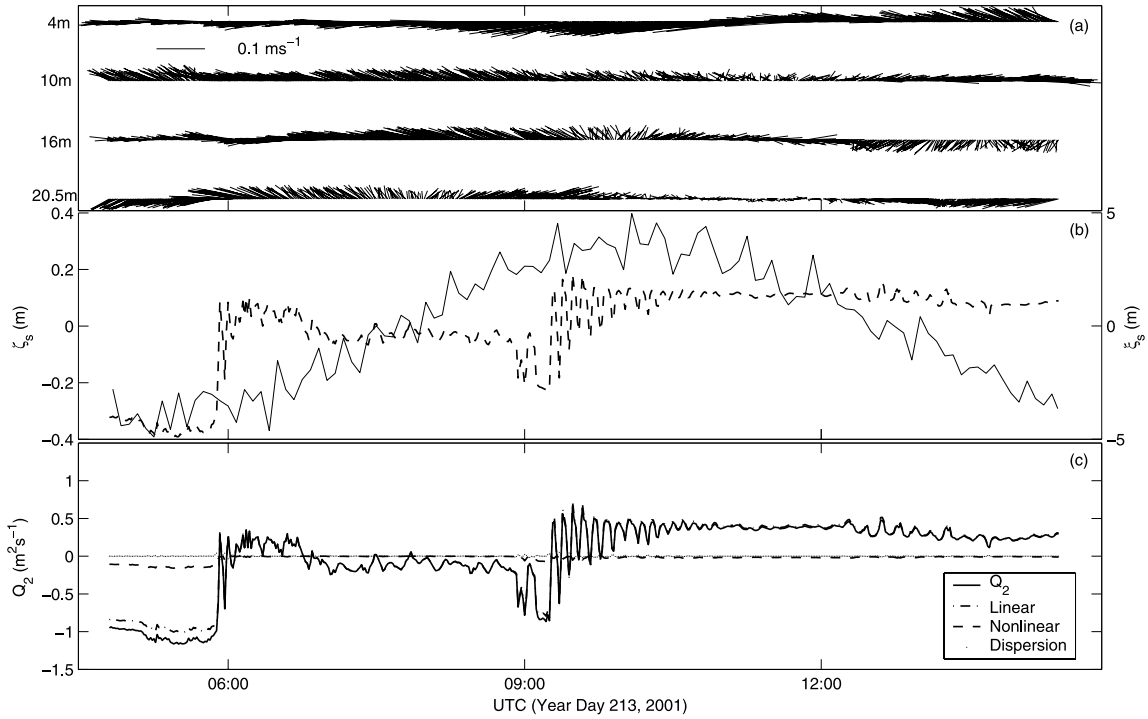

Figure 13. Time series of (a) baroclinic velocity vectors (U_{BC}) for the four levels of measurement of the water column, (b) barotropic tidal elevation (ζ_s, solid line) and 17°C isotherm displacement (χ_s, dashed line), and (c) Q_2 theoretical transport term at the SecNav mooring site from 0500–1400 UTC on year day 213, 2001.

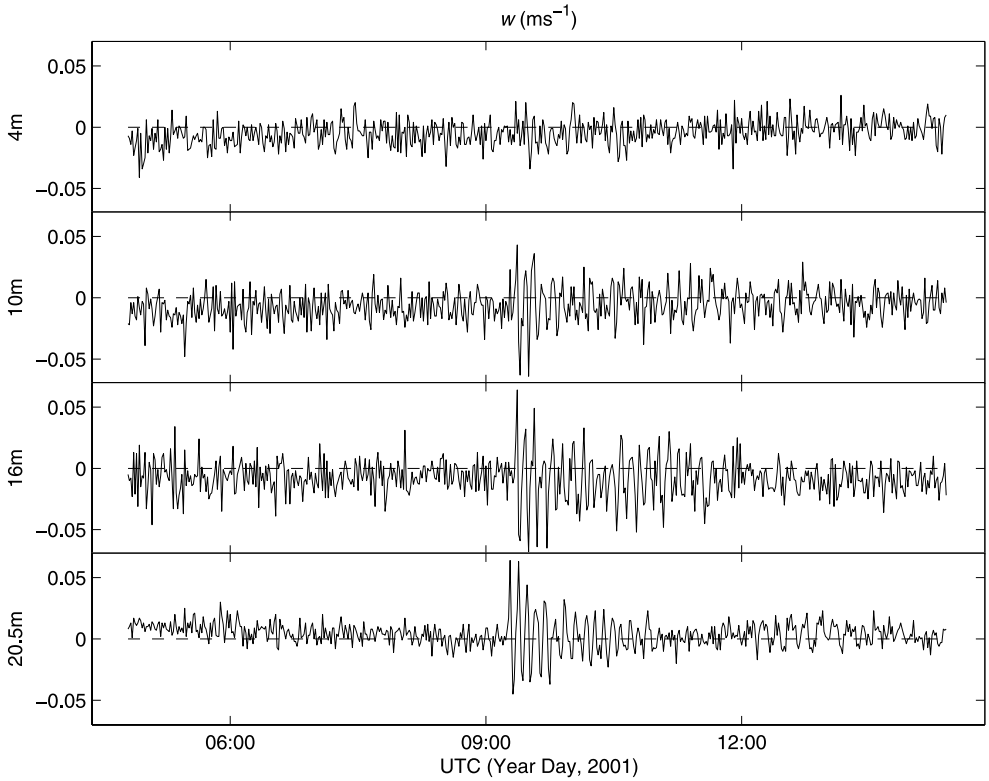

Figure 14. Vertical velocity, w, at four levels in the water column from 0500–1400 UTC on year day 213, 2001, at the SecNav mooring site.

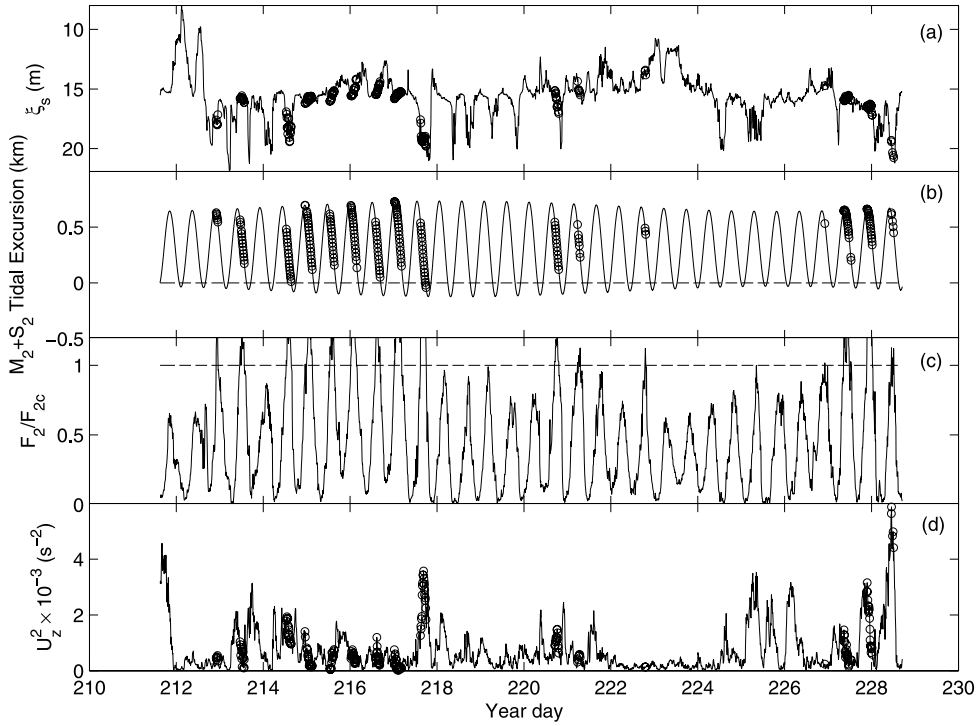

Figure 15. Time series of (a) vertical displacement of the 17°C isotherm, ξ_s (m), (b) M_2 and S_2 barotropic tidal excursion, (c) F_2/F_{2c}, and (d) shear, U_z^2, at the SecNav mooring site. Open circles are times of hydraulic control.

applied owing to the limited vertical resolution of velocity measurements.

[39] A lower layer critical Froude number, F_{2c}, modified after *Holloway* [1987] was used to identify critical flow in the lower water column,

$$F_{2c} = \left[1 + RV^2/(1-R)\right]^{-\frac{1}{2}}. \quad (6)$$

F_{2c} was estimated from: $R = h_2/H$, the ratio of lower layer depth relative to the seabed to total depth of the water column, and $V^2 = v_1^2/v_2^2$, where v_1 and v_2 are the across-shore baroclinic velocities in the upper and lower layer. Because values of R and V^2 are finite, jumps can occur when $F_{2c} < 1$. Thus flow actually comes under hydraulic control when $F_2/F_{2c} = 1$. The lower layer Froude number, $F_2^2 = v_2^2/g'h_2$, was calculated using $g' = g\ \Delta\rho/\rho_2$, the across-shelf velocity, v_2, with respect to linear mode 1 wave speed, $c_0 = N_0 H/\pi$, estimated from the mean buoyancy frequency over a total water depth, H, at each time increment.

[40] The results from the computation of F_2/F_{2c} are presented along with tidal excursion (computed from the M_2 and S_2 harmonic fit to the across-shelf barotropic velocity data) and the 17°C isotherm displacement, ξ_s (the deepest continuous isotherm at the SecNav site). Orientation of the tidal M_2 ellipse (325°T) computed from the barotropic current tidal fit showed the direction of tidal propagation toward the northeast during the flood phase, orthogonal to the local 30-m isobath. During the ebb phase, the tidal stream flowed toward the southwest. Undulations in ξ_s shown in Figure 15a coincided with the flood and ebb phase of the across-shelf tidal excursion, but the amplitude of ξ_s appeared insensitive to the Spring-Neaps cycle.

[41] The Froude number analysis at the study site shows that critical values of F_2/F_{2c} (times of occurrence shown by circles in Figure 15) only occurred after times of local high water on the ebb (off shelf) phase of the across-shelf tidal excursion as shown in Figure 15b. The corresponding vertical shear records, $U_z^2 = (\partial u_{BC}/\partial z)^2 + (\partial v_{BC}/\partial z)^2$, at 18.25 m (between the bottom and lower mid-water current meters) are presented in Figure 15d. The analysis shows that the magnitude of vertical shear before hydraulic control tended to increase. As the jump formed, the magnitude of vertical shear through the lower water column decreased. This hydraulic and vertical shear analysis effectively demonstrated the sudden transitions from stable to unstable conditions in the region of the SecNav mooring during tidal ebb conditions.

5.2. IWOE Coalescence

[42] This phase coupling of critical flow with the ebb tidal excursion posed an interesting question. Why, if the barotropic tide is advecting the entire water column past the mooring site, does super-critical hydraulic control only occur on the ebb off-shelf tidal excursion? Laboratory results from *Helfrich* [1992] and *Michallet and Ivey* [1999] suggest that shoaling internal waves on a sloping bed continue to propagate onto the inner shelf at the bottom boundary. This denser, cooler water eventually reaches a state of gravitational instability in the shallower inshore region. Gravitational relaxation of mass transported by previous bores or IWOEs then forces the lower layer to ''runback'' downshelf. On the retreat, the outflow gathers momentum until interacting with a later series of shoreward propagating IWOEs. This may result in reaching a state or level of hydrostatic

equilibrium and/or collision with later series of shoreward propagating IWOEs.

[43] It is also possible for this process to be further complicated by the superposition of across-shelf barotropic advection. For example, during the flood tide, the dense water driven by shoaling internal waves may be periodically trapped on shelf by barotropic forcing. Then, during the off-shelf tidal excursion, the shoaled water is released, runs back, and interacts with a secondary series of shoreward propagating IWOEs.

[44] Thus in this conceptual model of our observations, we first assume mass conservation and an upper rigid lid and solid bottom boundary condition at the seabed. The predicted flow coalescence between gravitational runback and the onshore propagating internal wave field would then require: a convergence in mass transport that eventually leads to a deepening of the lower layer, a convergence in horizontal velocity, and an increase in vertical velocities to maintain continuity.

[45] To explore this model, we first estimate the mass transport by the IWOEs at the SecNav mooring site through equation (7), which is based on a KdV assumption [*Inall et al.*, 2001]. By assuming no barotropic flux, the transport in the upper layer h_1 has the same absolute value (through mass conservation) as the transport Q_2 in the lower layer h_2. Therefore this estimate of transport by the IWOEs can be based on the time varying interfacial displacement of the two layers, ξ_s, and the linear phase speed, c_0, of the internal wave. Thus $Q_2 = +$ indicates a wave of elevation, and $Q_2 = -$ indicates a wave of depression. Equation (7) has also the added benefit of not being restricted to KdV type solitary waves.

$$Q_2 = c_0\left(\xi_s + \frac{3(h_2 - h_1)}{4h_1h_2}\xi_s^2\right) + \frac{h_1h_2}{6c_0}\frac{\partial^2\xi_s}{\partial t^2}. \qquad (7)$$

[46] Figure 13c shows lower layer transport, Q_2, computed for the period shown in Figure 9a from the mooring data. Transport estimates were dominated by the linear term. The nonlinear and dispersion terms were small and in near balance through the times of bore and IWOE propagation through the mooring site and thus were in good agreement with the KdV assumption for solitary waves.

[47] Q_2 estimates show an initial positive transport during passage of the first bore associated with the baroclinic velocity vectors, U_{BC}, in the lower water column being closely coupled with the barotropic tidal curve (Figure 13b) and directed in an onshore direction. Transport in the lower layer then reverted back to slightly negative values until the time of local high water.

[48] The second influx of cooler off-shelf water becomes apparent in mooring data some 3 hours later (approximately 0915 UTC) and was again accompanied by a positive increase in Q_2 along with a further deepening of the lower layer h_2. The larger nonlinear type fluctuations in the along-shelf velocity u_{BC} (see Figure 12) suggested that cooler bottom water was being transported alongshore at this stage of the flood tide. However, the total vector magnitude of horizontal flows shown in Figure 13a was very weak.

[49] The exact source of cooler bottom water and the direction of internal bore propagation using the results from single mooring time series data is speculative. Nevertheless, on the basis of the IR imagery, transport computation, the weak (vector) horizontal flow rates, and corresponding increases in vertical velocities (see Figure 14), there is a strong argument to suggest that internal waves or bores were orientated and coalesced in an across-isobath direction at the SecNav mooring site.

[50] Figure 14 shows the magnitude of vertical velocities, w, caused by the coalescence of flow in the water column as the upper layer abruptly shallowed for the second time. Vertical velocities of order 5–6 cm s^{-1} corresponded with the timing of horizontal flow convergence shown in Figure 16a. The estimated change in interfacial depth, ξ_{spred}, through the surge in the vertical component of flow was computed by integrating the vertical velocity w at the 20 m level between an initial limit, t_0, set at the onset of the vertical velocity surge and t_1, the end of the surge.

$$\xi_{spred} = \int_{t_0}^{t_1} w\,dt. \qquad (8)$$

[51] Results of the ξ_{spred} estimation computed from equation (8) as compared to the observed ξ_s are presented in Figure 16c. The predicted values of interfacial displacement from vertical velocity records show good agreement with the observed, emphasizing the coupled response of lower layer depth and velocity records. The slight positive over-prediction of vertical displacement from equation (8) results through the assumption of no vertical mixing through the lack of vertical shear (shown in Figure 15d) and hydrostatic damping.

[52] Some evidence of flow coalescence, although not as pronounced as on year day 213, was observed in data at times of critical flow, i.e., $F_2/F_{2c} \geq 1$ on approximately 50% of the observed ebb tidal excursions. Therefore this analysis is in reasonable agreement with the conceptual hydrodynamical model. Why the lack of hydraulic control on other ebb tides is not clear, and no direct link to local wind or tidally driven processes could be confidently established. We therefore have to submit to the fact that the complex inner shelf interaction between internal tidally driven bores, high-frequency IWOEs, stratification, and nonlinear inshore processes is complicated and all factors cannot be incorporated into our simple conceptual model. To fully understand the hydrodynamic trends of internal waves in very shallow waters would require several moorings in the region of flow coalescence caused by internal bore and IWOE propagation.

6. Source of Internal Bores

[53] Outstanding questions remain on the source of the higher-frequency waveform generation associated with the on- and off-shelf propagation of the inshore waveforms. Inner shelf topography has a gentle relief (see Figure 1b) and presents no steep bottom obstacles or obstructions likely of forming internal waves or hydraulic jumps as observed at the SecNav site. Therefore the main possible source of these inshore disturbances of the water column on periodic timescales is the internal tide.

[54] *Small* [2003] and *Orr and Mignerey* [2003] have recently observed internal wave shoaling. Earlier, the dynamics of internal wave shoaling on a uniform slope were investigated by *Helfrich* [1992] using a two-layer physical laboratory model. Through experimentation, a breaking criterion based on water column depth and soliton wave

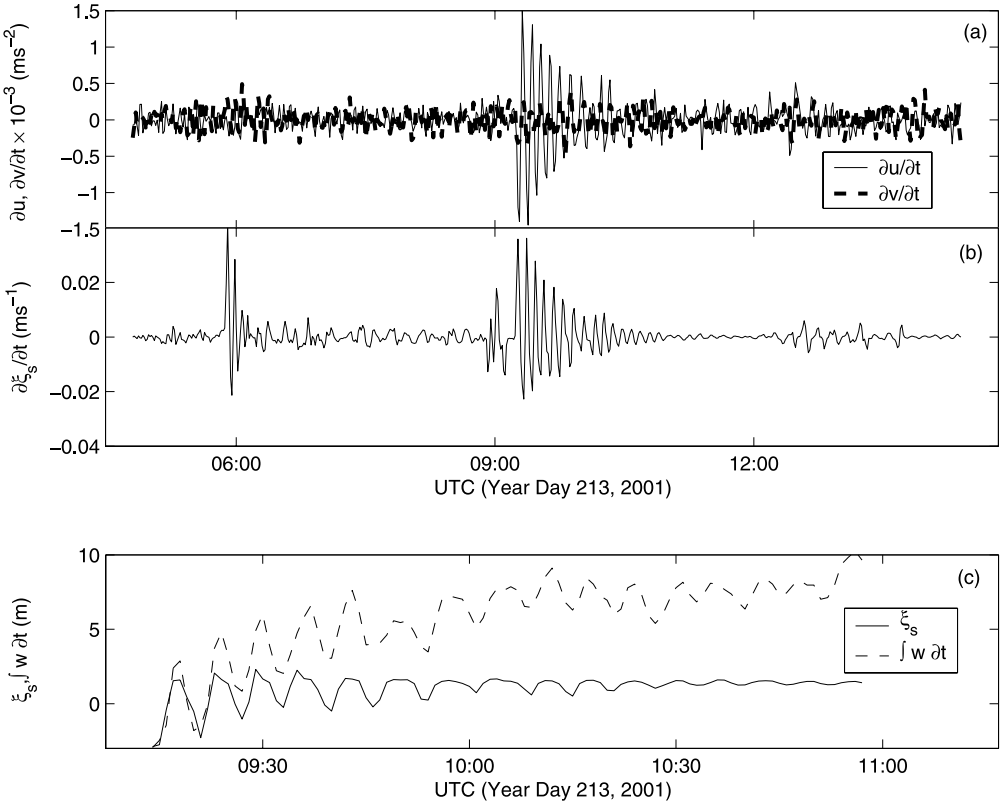

Figure 16. Time series of (a) horizontal velocity divergence/convergence of baroclinic velocities ($\partial u_{BC}/\partial t$, $\partial v_{BC}/\partial t$) at the 20.5 m level, (b) 17°C isotherm divergence/convergence ($\partial \zeta_s/\partial t$), and (c) 17°C isotherm displacement (ζ_s) and $\xi_{spred} = \int_{t_0}^{t_1} w\, dt$ from 0500–1400 UTC on year day 213, 2001, at the SecNav mooring site.

amplitude was derived to describe where a shoaling internal wave became weakly unstable and broke into a series of bolus-like instabilities. For

$$-a_0/z_s \lesssim 0.3, \tag{9}$$

where z_s is the total depth of fluid at a point on the sloping shelf, incident waves will move onshore with no instabilities. If

$$-a_0/z_u \gtrsim 0.4, \tag{10}$$

then z_u is the depth where the incident wave is unstable and characterized through strong overturning and second mode wave generation. By rearranging the two equations, we estimated from the offshore soliton amplitude, a_0 = 15 m, the approximate transition zone where internal waves generated on the outer shelf start to interfere with the bottom topography, become unstable, and eventually break. Extrapolation of z_s onto the across-shelf bathymetry predicts the start position of bottom boundary effects as 3.5 km south of the CBLAST mooring site in 50 m of water. The predicted point of wave overturning at z_u at a depth of 37.5 m is some 15 km south of the inshore SecNav mooring. Thus, according to laboratory experiments, the 18-km region in between z_s and z_u shown in Figure 1b is where internal waves undergo radical change from a predominately upper ocean to bottom boundary manifestation of the solitary waveforms coupled to the internal tide.

[55] Because of the limited spatial coverage of our data, it was not meaningful to try and determine a direct relationship between the timing of specific individual internal waves at the two mooring sites. However, it was possible to estimate through times series analysis a measure of the covariance between the internal tidal signal on the outer shelf to that on the inner shelf at specific frequency lags based on several quantifiable assumptions. First, we assume internal waves propagate onshore at a phase speed of $O(c_1)$. Second, it is postulated that the majority of variance associated with the vertical displacement of isotherms at each mooring site is dominated by the baroclinic tide. From a distance of 41 km between the two moorings and an internal wave phase speed of 0.33 m s^{-1}, the estimated time for arrival at the inshore site is approximately 34.5 hours.

[56] Results from the cross-correlation analysis between mooring isotherm displacements is presented in Figure 17. Arrows indicate the specific M_2, S_2, K_1, $2\pi/f$, and beat period frequency bands. In addition, the estimated time for a soliton detected at the offshore CBLAST mooring site to arrive at the inshore SecNav site is also shown in the figure. For lags in the range of ±10 hours, correlation between the two mooring sites was barely significant at the 99% confidence level. At greater ± time lag intervals, by far the greatest majority of higher cross-correlation values were all negative (displacements 180° out of phase) and at negative lags (inshore displacements lagging offshore dis-

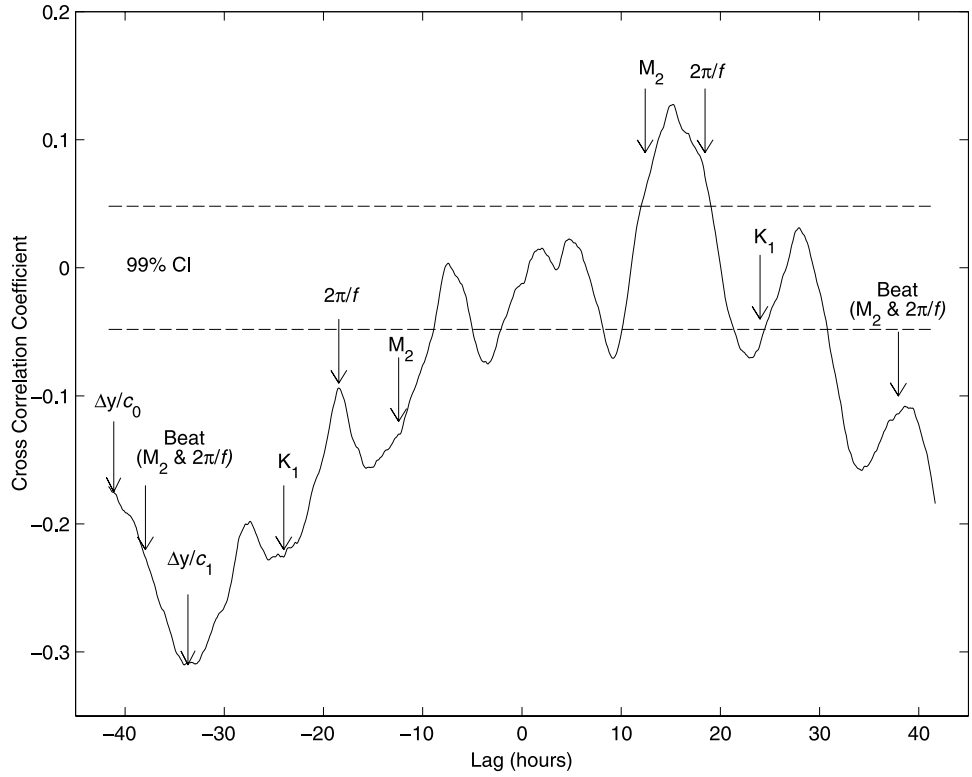

Figure 17. Lag cross-correlation analysis of isotherm displacements (m) between the CBLAST (ξ_c) and SecNav (ξ_s) mooring sites. Specific tidal, inertial, beat frequencies, and predicted time taken to travel between moorings, are shown at the appropriate lags.

placement). Positive coefficients (in phase displacement) with positive lags were centered in the M_2 tidal and inertial frequency band and probably produced by local wind and atmospheric driven events. The highest correlation of $O(-0.30)$ was estimated at a lag of 33 hours, close to the predicted time according to the nonlinear theory for an oscillation on the interface to travel between mooring sites.

[57] We accept that owing to the physical assumptions made from our data set, the lags in isotherm displacement between mooring sites are subject to some degree of uncertainty. Nevertheless, the physical interpretation of the cross-correlation analysis based on the estimated phase speed of internal wave propagation was founded in arguments derived from observational evidence and not mere conjecture. Therefore this analysis tentatively supports the laboratory studies and intuitive notion that extreme internal wave events present in the surface layer on the outer shelf were partly responsible for the bores and perturbations observed in the lower layer of the water column nearer inshore on the New England shelf region.

7. Discussion

[58] The results from this study of the inner New England shelf have identified a complex combination of longer period atmospheric forcing and shorter term tidal processes responsible for day to day changes in properties of the water column during a summer month. Coastal Ekman dynamics plus the anomalous fresh water inputs on the inner shelf ultimately control the longer period trends in the observed structure of the water column. However, the semi-diurnal periodic changes in stratification introduced by baroclinic tides, nonlinear solitary wave packets, and internal tidal bores add a further dimension to the problem of understanding the inner shelf summer time dynamics.

[59] We suggest from our temporally high resolution but spatially sparse data that internal tidal processes on the outer shelf play an important role in regulating and changing stratification on the inner shelf region. This notion may be supported by past investigations by *Helfrich and Melville* [1986] and the recent modeling studies of *Vlasenko and Hutter* [2002] and *Legg and Adcroft* [2003]. Results from their simulations suggest that upslope and onshelf propagating bores form through shoaling and interaction of the internal tide with the continental shelf. Steep slopes produce inshore propagating turbulent bores whereas gentle slopes as discussed in this study encourage the formation of steep bore fronts followed by dispersive internal waveforms.

[60] *Lentz and Trowbridge*'s [1991] examination of observations made on the northern California shelf suggested that upslope across-shelf transport carried denser bottom water inshore and increased stratification. Downslope transport carried heavier water under lighter water and tended to increase bottom boundary layer effects and mixing in the lower water column. These observations described transport under longer period upwelling and downwelling timescales.

[61] At the Martha's Vineyard site, a similar type of modulated stratification and bottom boundary layer growth

was also observed on much shorter semi-diurnal timescales. This was characterized by an onshelf deepening of the cooler lower layer of the water column during the flood phase of the tide. The inshore dynamics influenced by atmospheric forcing and freshwater input can cause complicated and possibly localized changes in the structure of the water column at the SecNav site. The hydraulic analysis and a comparison of our observations with an internal wave shoaling and breaking criterion proposed by *Helfrich* [1992] suggested internal waves propagating upslope and onshore from the outer shelf shoaled and continued to run up into the inner shelf region along the bottom boundary layer.

[62] During the ebb tide, a combination of across-shore and alongshore currents and a gravitational relaxation of the dense lower water column previously forced onshore by internal bores on the flood tide runbacks off shelf during the ebb tide. This offshore directed flow coalesces with further packets of incoming onshelf propagating internal waves of elevation. The convergence zone effectively forces an upwelling of cooler dense water, and increases the Froude number to critical values that in turn may stimulate an increased level of turbulent vertical mixing.

[63] *Winant and Olson* [1976] suggest that turbulent mixing occurs at the front of these types of surges and decays some distance behind the head owing to stabilization by stratification. This process was clearly shown in our results and in many of the classical laboratory studies of gravity type currents [e.g., *Simpson*, 1982]. Thus the overall effect of hydraulic control is to deepen the upper layer and decrease the overall potential energy state of the water column at the end of the ebb tide. Convergence suggests that cooler water through mass continuity would be forced up into the water column, as the laboratory experiments of *Michallet and Ivey* [1999] suggest, producing the cooler water temperature anomalies present in the IR imagery.

[64] The hypothesis presented by *Klymack and Moum* [2003], who suggest an ''irreversible'' transport of fluid properties in the nearshore is not clearly supported by our observations. In contrast, this analysis supports the notion of a low-energy oscillatory migration of the lower layer across the inner shelf. However, this may be a product of high internal tidal energy dissipation across the broad inner New England shelf and the low wind conditions that promote an enhanced vertical stratification through strong surface heating during the summer months. *Helfrich* [1992] also noted a continual back flow near to the base of the onshore flowing lower denser layer. Our observations could not resolve this feature of the flow although through continuity constraints it very likely exists. This hypothesis could be further verified and tested through the use of a closely spaced across-shelf current meter array.

[65] A direct method of estimating where and when there is hydraulic control at the inshore region of the shelf remains ambiguous. Froude number analysis showed that bores became supercritical on the ebb tide but failed to disclose a direct link between tidal phase, i.e., Spring or Neap tides, and inshore internal bores. However, jumps mainly occurred during upwelling favorable, light wind conditions. This coincided with strong stratification and internal tidal signatures at the offshore mooring site. A detailed examination of the results from a more recent longer running experiment is part of ongoing research.

[66] **Acknowledgments.** We wish to thank Jason Gobat, Chris Zappa, Andy Jessup, Tim Crawford, and Jerry Cressenti for their contributions to this study. The Woods Hole Oceanographic Upper Ocean Processes Group technical support staff and also the Mooring and Rigging Shop staff all made this work possible. We wish to also thank Captain Matt Stommel and the crew of FV *Nobska* for several successful cruises and efficient mooring operations during the CBLAST-Low pilot study. We are also grateful to two reviewers for critical and helpful comments. This work was funded by the Office of Naval Research under grant N00014-99-1-0029 and Secretary of the Navy/CNO Chair grant N00014-99-1-0090 to R. A. W. WHOI contribution 11198.

References

Apel, J., L. Ostrovsky, and Y. Stepanyants (1995), Internal solitons in the ocean, *Rep. MERCIRA0695*, Appl. Phys. Lab., Johns Hopkins Univ., Baltimore, Md.

Colosi, J., R. Beardsley, J. Lynch, G. Gawarkiewicz, C.-S. Chiu, and A. Scotti (2001), Observations of nonlinear internal waves on the outer New England continental shelf during the summer Shelfbreak Primer study, *J. Geophys. Res.*, *106*, 9587–9601.

Helfrich, K. (1992), Internal solitary wave breaking and run-up on a uniform slope, *J. Fluid Mech.*, *243*, 133–154.

Helfrich, K., and W. Melville (1986), On long non-linear internal waves over slope-shelf topography, *J. Fluid Mech.*, *167*, 285–308.

Holloway, P. (1987), Internal hydraulic jumps and solitons at a shelf break region on the Australian north west shelf, *J. Geophys. Res.*, *92*, 5405–5416.

Inall, M., G. Shapiro, and T. Sherwin (2001), Mass transport by non-linear internal waves on the Malin shelf, *Cont. Shelf Res.*, *21*, 1449–1472.

Klymack, J., and J. Moum (2003), Internal solitary waves of elevation advancing on a shoaling shelf, *Geophys. Res. Lett.*, *30*(20), 2045, doi:10.1029/2003GL017706.

Lamb, K. (1994), Numerical experiments of internal wave generation by stong tidal flow across a finite amplitude bank edge, *J. Geophys. Res.*, *99*, 843–864.

Lamb, K., and L. Yan (1996), The evolution of internal wave undular bores: Comparsions of a fully nonlinear numerical model with weakly nonlinear theory, *J. Phys. Oceanogr.*, *26*, 2712–2734.

Lee, C.-Y., and R. Beardsley (1974), The generation of long nonlinear internal waves in a weakly stratified shear flow, *J. Geophys. Res.*, *79*, 453–462.

Legg, S., and A. Adcroft (2003), Internal wave breaking at concave and convex continental slopes, *J. Phys. Oceanogr.*, *33*, 2224–2246.

Lentz, S., and J. Trowbridge (1991), The bottom boundary layer over the northern California shelf, *J. Phys. Oceanogr.*, *21*, 1186–1201.

Lentz, S., R. Shearman, S. Anderson, A. Plueddemann, and J. Edson (2003), The evolution of stratification over the New England shelf during Coastal Mixing and Optics study, August 1996 to June 1997, *J. Geophys. Res.*, *108*(C1), 3008, doi:10.1029/2001JC001121.

MacKinnon, J., and M. Gregg (2003), Mixing on the late-summer New England shelf—Solibores, shear, and stratification, *J. Phys. Oceanogr.*, *33*, 1476–1492.

Michallet, H., and G. Ivey (1999), Experiments on mixing due to internal solitary waves breaking on uniform slopes, *J. Geophys. Res.*, *104*, 13,467–13,477.

Orr, M. H., and P. C. Mignerey (2003), Nonlinear internal waves in the South China Sea: Observation of the conversion of depression internal waves to elevation internal waves, *J. Geophys. Res.*, *108*(C3), 3064, doi:10.1029/2001JC001163.

Pineda, J. (1999), Circulation and larval distribution in internal tidal bore warm fronts, *Limnol. Oceanogr.*, *44*, 1400–1414.

Pritchard, M., J. Gobat, W. Ostrom, J. Lord, P. Bouchard, and R. Weller (2002), CBLAST-Low 2001 Pilot Study: Mooring deployment cruise and data report; FV *Nobska*, June 4 to August 17, 2001, *Tech. Rep. WHOI-2002-03*, 61 pp., Woods Hole Oceanogr. Inst., Woods Hole, Mass.

Rippeth, T., and M. Inall (2002), Observations ot the internal tide and associated mixing across the Malin shelf, *J. Geophys. Res.*, *107*(C4), 3028, doi:10.1029/2000JC000761.

Shearman, R., and S. Lentz (2003), Dynamics of mean and subtidal flow on the New England shelf, *J. Geophys. Res.*, *108*(C8), 3281, doi:10.1029/2002JC001417.

Shearman, R. K., and S. J. Lentz (2004), Observations of tidal variability on the New England shelf, *J. Geophys. Res.*, *109*, C06010, doi:10.1029/2003JC001972.

Simpson, J. (1982), Gravity currents in the laboratory, atmosphere and ocean, *Annu. Rev. Fluid Mech.*, *14*, 213–234.

Small, J. (2003), Refraction and shoaling of nonlinear internal waves breaking at the Malin shelf break, *J. Phys. Oceanogr.*, *33*, 2657–2674.

Stanton, T., and L. Ostrovsky (1998), Observations of highly nonlinear solitons over the continental shelf, *Geophys. Res. Lett.*, *25*, 2695–2698.

Vlasenko, V., and K. Hutter (2002), Numerical experiments on the breaking of solitary internal waves over a slope-shelf topography, *J. Phys. Oceanogr.*, *32*, 1779–1793.

Winant, C. (1974), Internal surges in coastal waters, *J. Geophys. Res.*, *79*, 4523–4526.

Winant, C., and J. Olson (1976), The vertical structure of coastal currents, *Deep Sea Res.*, *23*, 925–936.

Zappa, C., and A. T. Jessup (2005), High resolution airborne infrared measurements of ocean skin temperature, *Geosci. Remote Sens. Lett.*, *2*(2), doi:10.1109/LGRS.2004.841629.

M. Pritchard, Institute for Atmospheric Science, School of Earth and Environment, University of Leeds, Leeds LS2 9JT, UK. (mp@env.leeds.ac.uk)

R. A. Weller, Department of Physical Oceanography, Woods Hole Oceanographic Institute, Woods Hole, MA 02543, USA. (rweller@whoi.edu)